Determination of band offsets in strained $In_xGa_{1-x}As/GaAs$ quantum wells by capacitance-voltage profiling and Schrödinger-Poisson self-consistent simulation

V. I. Zubkov,* M. A. Melnik, A. V. Solomonov, and E. O. Tsvelev
St. Petersburg Electrotechnical University "LETI," Prof. Popov str. 5, 197376, St. Petersburg, Russia

F. Bugge, M. Weyers, and G. Tränkle
Ferdinand-Braun-Institut für Höchstfrequenztechnik, Albert-Einstein-Str. 11, D-12489 Berlin, Germany
(Received 6 May 2004; published 25 August 2004)

The results of capacitance-voltage profiling and numerical simulation of charge carrier distribution and energy states for strained quantum wells $In_xGa_{1-x}As/GaAs$ $(0.06 \leqslant x \leqslant 0.29)$ are presented. Precise values of conduction band offsets for these pseudomorphic QWs have been obtained by means of self-consistent solution of Schrödinger and Poisson equations and following fitting to experimental data. For the conduction band offsets in strained $In_xGa_{1-x}As/GaAs$-QWs the expression $\Delta E_C(x) = 0.85x - 0.3x^2$ has been obtained.

DOI: 10.1103/PhysRevB.70.075312 PACS number(s): 73.21.Fg, 81.07.St

I. INTRODUCTION

Since the development of semiconductor heterostructures the determination of energy band discontinuities of various semiconductor pairs has been a very important task. Energy band offsets dominantly control the electronic states in heterostructures and, hence, the output parameters of devices. The importance of getting true values of band offsets as well as the difficulties in obtaining and, even more, in interpreting the relevant data have been attracting attention for the last 30 years. Dingle was one of the first who reported in 1974–1975 (Ref. 1 and 2) the value of band offsets for the isoperiodic heterosystem (Al-Ga)As/GaAs ("Dingle" rule 85:15). Then Kroemer,[3–5] Duggan,[6] and Yu *et al.*[7] reviewed in detail the understanding of band offsets before 1991 and provided an overview of the methods commonly used in experimental band offset determination, mostly optical at that time. At the same time, the authors[8] and others showed that a low sensitivity of the optical transition energies to the band offsets made its determinations rather confusing. Up to now a great number of papers has been published on this subject (see bibliography in recent comprehensive review[9]). So far, however, as was pointed out in the review, among the ternary alloys used in quantum electronics, only the AlGaAs/GaAs system has generally accepted values of band offsets.

For one of the most important used heteropairs—$In_xGa_{1-x}As/GaAs$—as yet no clear picture about the dependence of band offsets on alloy composition has been obtained, despite the intensive investigations in the last years. The data collected by Bhattacharya[10] show a great scatter of the values of relative conduction band offset ΔE_C between 35% and 85% for $x < 0.35$. Above mentioned review[9] reports relative conduction band offsets for the $In_xGa_{1-x}As/GaAs$ system in the range 57%–90% and recommends the compositional dependence for ΔE_C, which may be estimated approximately as $\Delta E_C(\mathrm{eV}) = 0.96x - 0.1x^2$. They conclude that no detailed study has yet been carried out on InGaAs-based heterojunctions. Recent publications on this subject[11–14] only present partial results for different compositions, more or less agreed with "recommended" in Ref. 9. Theoretic calculations[15] give the valence band offset for the end combination InAs/GaAs $\Delta E_V = 0.06$ eV, which is in serious disagreement with experimental data.

One important device application of the heterosystem InGaAs/GaAs is high power laser diodes with strained quantum wells.[16] In these structures thin quantum-size layers of InGaAs grow pseudomorphically, i.e., having the lattice constant of the underlying GaAs-layer in the plane of the heterojunction. The elastic energy, accumulated due to crystal cell distortion, causes the band structure of the thin InGaAs layer to be modified,[17] altering particularly its forbidden energy gap. Hence, in strained InGaAs/GaAs quantum wells one should expect another band offsets than in heterostructures with thick layers of the solid solution. In cases between pseudomorphic growth and full strain relaxation (occurs in thick layers) the band offset in InGaAs/GaAs will have, obviously, some intermediate values. This fact explains, we suppose, the variety of data found in the literature on this heterosystem. The second source of errors and contradictions are simplified models for interpretation of the experimental data, particularly the neglect of quantization effects.

Numerical fitting of capacitance-voltage (C-V) curves[11,18–20] is one of the most promising approaches to measure band offsets in quantum well (QW) structures. The C-V-fitting by means of self-consistent solution of Schrödinger and Poisson equations correctly takes the quantization of carriers in quantum well into consideration and yields very accurate results.[19,21] However, well-defined heterostructures are necessary for this.

Complex multilayer structures like multi-QWs, superlattices etc. and unknown dopant profile or the presence of deep levels add sources of uncertainties. Therefore, in order to be sure to get precise values for band offsets at heterojunction simple structures with a minimum of unknown parameters or parameters to be fitted should be used.

This work presents accurate data for band offsets in heterostructures with strained pseudomorphic $In_xGa_{1-x}As/GaAs$ $(0 < x < 0.3)$ quantum wells. To obtain these values we have carried out a systematic cycle of C-V-measurements on specially fabricated structures. Details of sample preparation and

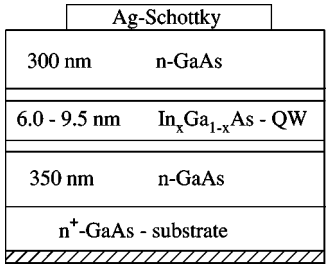

FIG. 1. The layer sequence of the grown samples with $In_xGa_{1-x}As/GaAs$ quantum wells.

measurements are described in Sec. II. In Sec. III the model for simulating measured concentration profiles and deriving the values of conduction band offsets based on self-consistent numerical solution of the Schrödinger and Poisson equations is described. The carrier concentration in the quantum well region is calculated on the base of a quantum-mechanical approach. Mathematical aspects of the computations are presented in Secs. III A and III B. To increase the accuracy of numerical calculations a nonuniform mesh with the mesh step inside the quantum well 10 times smaller than in the other regions has been used. Finally, in Sec. IV we present the results of numerical fitting of experimentally measured *C-V* curves. The dependence of conduction band offset for strained pseudomorphically grown $In_xGa_{1-x}As/GaAs$-QWs has been obtained as a function of quantum well composition in the range $0.06 \leqslant x \leqslant 0.29$.

II. SAMPLE STRUCTURE AND MEASUREMENT PROCEDURE

A special set of high quality samples with a simplified structure (Fig. 1) containing $In_xGa_{1-x}As/GaAs$ quantum wells of different width ($w=6.0-9.5$ nm) and composition ($x=0.065-0.29$) was grown on n^+-GaAs substrates by metal-organic vapor phase epitaxy (MOVPE) at deposition temperatures of 650 °C and 770 °C. The GaAs cladding layers were uniformly doped with Si, except for the QWs themselves and thin (5 nm) spacer layers on both sides of the quantum well. The introduction of undoped spacers around QW is, from our point of view, the optimal compromise between the total simplification of the structure to be measured and the desire to maintain the active zone as in real device with strained quantum well. Their presence is easily taken into account during *C-V*-simulations. To get the best experimental results and to eliminate possible uncertainties in the subsequent numerical fitting, the cap GaAs layer was designed to be 300 nm thick and have a constant doping level $(6-7)\times 10^{16}$ cm^{-3}. The width and composition of the QWs and cladding layers have been determined by high resolution x-ray diffraction (HRXRD). All QWs were fully strained without any relaxation seen in x-ray area maps.[16] The accuracy of fitting the experimental rocking curves using the Epitaxy 4 software of PANalytical was ±1 nm for cap layer and better than ±0.5 nm for QW. The composition was calculated from the perpendicular lattice parameter assuming that the QW was pseudomorphically strained. The accuracy of composition determination was ±0.005. Ag-Schottky barriers were fabricated on top of the structures and Ohmic contacts were formed on the substrate.

The parameters of the grown structures are listed in Table I.

The measurements of capacitance-voltage characteristics and profiling of majority carriers in the quantum wells have been carried out with the help of a computer-controlled *C-V*-profilometer at testing frequency 1 MHz and with the amplitude of the probing signal 15 or 50 mV.

At zero bias the width of the space charge region under the Schottky-barrier in the samples was less than the thickness of the cap GaAs-layer. With increasing reverse bias the space charge region was broadened and its border crossed the quantum well. The *C-V*-characteristics of all samples clearly exhibit a plateau in the range of $U_{rev}=2-4.5$ V related to discharging carriers in the QW. A typical example of

TABLE I. Characteristics of the structures and results of numerical simulation of conduction band discontinuities in $In_xGa_{1-x}As/GaAs$ strained quantum wells grown by MOVPE.

Sample No.	x	T deposition (°C)	d cap layer (μm)	QW width (nm)	E of bound level at 0 V (meV)	ΔE_C (meV)
298	0.065	770	0.304	9.5	−10.9	55
299	0.14	770	0.304	8.0	−29.0	110
308	0.145	650	0.302	6.0	−25.0	110
303	0.145	650	0.305	7.5	−32.1	120
309	0.145	650	0.302	9.5	−35.1	120
296	0.19	770	0.295	6.5	−38.3	150
297	0.2	650	0.298	6.5	−39.5	155
306	0.215	770	0.304	7.2	−43.7	160
307	0.225	770	0.308	7.4	−48.8	175
300	0.23	770	0.304	7.2	−48.5	175
301	0.27	770	0.300	6.5	−54.6	210
305	0.29	650	0.300	6.0	−55.3	220

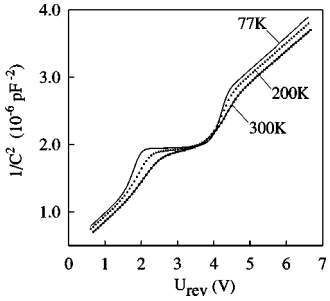

FIG. 2. *C-V*-characteristics of $In_{0.225}Ga_{0.775}As/GaAs$-QW at different temperatures (sample #307).

$1/C^2 = f(U_{rev})$ characteristic for sample #307 at different temperatures is shown in Fig. 2.

The apparent carrier distribution was derived from a measured *C-V* curve using the well known formula for the full depletion approximation[22]

$$n(d) = -2\left[\epsilon\epsilon_0 eA^2 \frac{d}{dV}\left(\frac{1}{C^2}\right)\right]^{-1}, \tag{1}$$

where ϵ is the dielectric constant (assumed to be equal for both the well and the barriers), e is the electron charge, A is the area of the Schottky diode. The depletion width d was given as usual by

$$d = \frac{\epsilon\epsilon_0 A}{C}. \tag{2}$$

Figure 3 shows some examples of $n-d$ curves covering the whole range of QW compositions. The profiles exhibited clear dependence of amplitude, width, and the depth of depletion on the composition and the width of the QWs. It is worth noting that beyond the regions of accumulation and depletion related to the QW the carrier concentration was excellently constant, and we used it in the fitting of the experimental profiles to the simulated ones on the base of self-consistent solution of the Schrödinger and Poisson equations by varying the band offset.

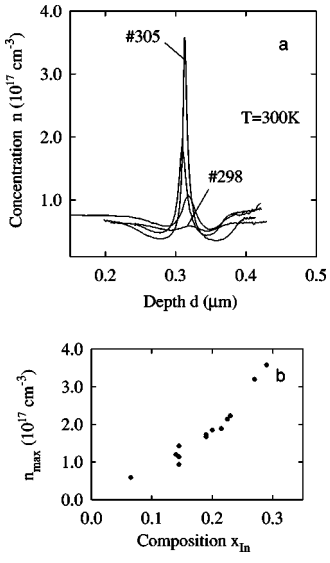

FIG. 3. *C-V*-profiling of $In_xGa_{1-x}As/GaAs$ quantum wells. Samples #296–#309. (a) Common view of apparent carrier concentrations for several samples; (b) apparent concentration peak values as a function of x. Note that near $x=0.14$ there are 4 samples with different width of QW.

III. MODEL FOR SIMULATING *C-V* PROFILES

For simulating the *C-V*-characteristics the Poisson equation

$$\frac{d}{dz}\left(\epsilon_0\epsilon(z)\frac{d\varphi(z)}{dz}\right) = e[N_D^+(z) - n(z)] \tag{3}$$

has been solved, where $\varphi(z)$ is the electrostatic potential, $n(z)$ is the free carrier concentration, and N_D^+ is the concentration of ionized donors. The boundary conditions for (3) at the Schottky barrier and in the electroneutrality region, far away from the QW, are

$$\varphi(0) = U + \varphi_{bi}, \tag{4}$$

$$\varphi(\infty) = 0. \tag{5}$$

Here U is the applied voltage, and φ_{bi} is the built-in potential.

In addition, the matching conditions for the potential at both heterointerfaces have to be fulfilled,

$$\epsilon_{barr}\frac{d\varphi_{barr}}{dz} = \epsilon_{well}\frac{d\varphi_{well}}{dz}. \tag{6}$$

The indexes "barr" and "well" correspond to the regions of GaAs barrier and InGaAs quantum well, respectively.

The free carrier concentration $n(z)$ in (3) far from the QW can be calculated as in the case of a homogeneous bulk structure through the Fermi integral[22]

$$n(z) = N_C\frac{2}{\sqrt{\pi}}F_{1/2}\left(-\frac{E_C - E_F - e\varphi(z)}{kT}\right), \tag{7}$$

where N_C is the effective density of states in the conduction band, E_F is the Fermi level, T is the temperature, and k is the Boltzmann constant. In contrast, in the vicinity of a quantum well the carrier concentration should be calculated by solving Schrödinger's equation. We derived the needed spatial distribution of the electrostatic potential using a procedure of self-consistency of the Schrödinger and Poisson equations. The essence of the procedure is the sequential (step-by-step) solution of Schrödinger and Poisson equations until convergence.[23–25] As a criterion of convergence we took the increment of the potential less than 10^{-8} V at the next iteration.

Quantum size effects are important only inside quantum well and in its immediate vicinity. Therefore, for numerical solution of the Schrödinger equation we used a "quantum box"—a narrow region containing the QW (Fig. 4). The optimal width of the quantum box was chosen experimentally during simulations, in order to achieve high precision in determination of the quantized carrier concentration, and, in balance, to reduce the computation time. The quantum box

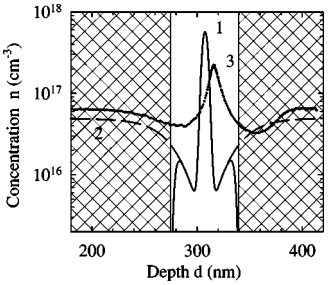

FIG. 4. Scheme of computations. The "quantum box" is unshaded. 1, Schrödinger's concentration; 2, concentration derived from Eq. (7); 3, resulting calculated "apparent" carrier concentration (matched the experiment).

width was chosen as nine times the width W of the corresponding quantum well, which was placed in the center of the quantum box.

According to the boundary conditions, there must be nodes of the wave functions at the edges of the quantum box. For this reason the data calculated close to the quantum box boundaries are dropped. The length of this region is no more than 1 W, as can be seen from Fig. 4. On the other hand, at distances about $2-3$ W from the QW the quantization effect is very weak, and there we can use the Fermi integral (7) for deriving the free carrier concentration. The coincidence of the concentration profiles at this part, derived from the quantum-mechanical approach and from (7), was used as the proof for a true solution.

A. Solving the Poisson equation

The Poisson equation has been solved numerically by Newton's method relative to the correction term.

The great difference (tenfold) in the values of electron and hole effective masses in GaAs and nearby ternary InGaAs alloys makes the Fermi level shift toward the bottom of the conduction band. Therefore, a significant part of donors (up to 30%) remains nonionized at room temperature, even despite the very low ionization energy of Si donors in GaAs [about 5 meV (Ref. 26)]. Because of this, the incomplete donor ionization has to be taken into account.

To reduce the computation time, it is desirable to use some approximation of the Fermi integral (7). The simplest exponential approximation is not applicable here because of the close position of the Fermi level to the bottom of the conduction band. There is another well known approximation for (7) by the expression

$$n(z) = \frac{N_C}{C_n + \exp\left(\dfrac{E_C - E_F - e\varphi(z)}{kT}\right)} \tag{8}$$

that better matches the Fermi integral. The constant C_n here usually falls between 0.17 and 0.35.[27]

In order to minimize the approximation error and to fulfill the electroneutrality condition on the right-hand side of the simulated region (i.e., in the GaAs substrate) we used the following procedure: by solving the electroneutrality equation and using expression (7) the Fermi level position is determined at $\varphi=0$. Then equating (7) to (8) one can derive the current adaptivity constant C_n. At another φ the maximum relative error of such approximation does not exceed 3×10^{-4}. Such an approach reduces the computation time more than on the order without any loss in accuracy.

The electrostatic potential was written as an initial approximation $\varphi_0(z)$ and a correction term $\Delta\varphi(z)$:

$$\varphi(z) = \varphi_0(z) + \Delta\varphi(z). \tag{9}$$

To linearize the Poisson equation (3) the expression for n was decomposed into a Taylor series including linear term relative to the correction $\Delta\varphi(z)$.

Then a finite-difference analog of the Poisson equation has been rewritten as a system of linear equations with a characteristic three-diagonal form. To get a high precision solution in a reasonable time different mesh steps were used inside and outside the quantum box. The number of points in the mesh was 8000, including about 1500 in the quantum box. The Gauss method was applied to solve the system with some modifications based on obvious symmetry of the equations.

After getting the correction $\Delta\varphi(z)$ a new potential was obtained according to (9).

B. Solving the Schrödinger equation

The effective mass, one-dimensional Schrödinger equation can be written as[24]

$$-\frac{\hbar^2}{2}\frac{d}{dz}\frac{1}{m^*(z)}\frac{d\psi_i(z)}{dz} + V(z)\psi_i(z) = E_i\psi_i(z), \tag{10}$$

where E_i are the eigenvalues, ψ_i are the corresponding eigenvectors, m^* is the coordinate-dependent electron effective mass. $V(z)$ is the effective potential energy,

$$V(z) = \begin{cases} e\varphi(z) + \Delta E_C & \text{inside QW}, \\ e\varphi(z) & \text{outside QW}. \end{cases} \tag{11}$$

ΔE_C is the conduction band offset.

The boundary conditions of Dirichlet's type $\psi(0)=\psi(N)=0$ are hold at the quantum box edges.

The finite-difference analog for (10) was obtained using the three-point formula

$$-\frac{\hbar^2}{2m_j^*}\frac{\psi_{i,j-1} + \psi_{i,j+1} - 2\psi_{i,j}}{h_j^2} + V_j\psi_{i,j} = E_i\psi_{i,j}, \tag{12}$$

where j identifies the point in the one-dimensional mesh, and h_j is the distance between the mesh nodes (a step of the mesh).

In addition to boundary conditions, at the heterojunctions the following matching conditions should be maintained between the derivative of wave functions inside and outside the quantum well,

$$\frac{1}{m^*_{\text{barr}}}\frac{\Delta\psi_{\text{barr}}}{h_{\text{barr}}} = \frac{1}{m^*_{\text{well}}}\frac{\Delta\psi_{\text{well}}}{h_{\text{well}}}. \tag{13}$$

Then the discretized analog for the Schrödinger equation (12) was solved numerically by well known "shooting"

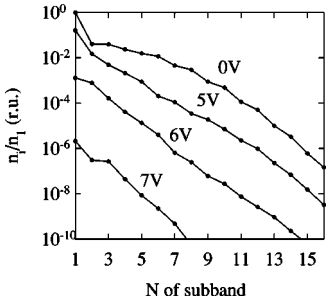

FIG. 5. Electron concentration in first 16 energy subbands (relatively to the concentration in the first subband) at different reverse biases. Sample #300 (ΔE_C=175 meV), T=300 K.

method with some improvements to reduce the computation time.

The number of points in the mesh should be enough to eliminate the error due to substitution of the derivative with the finite-difference approximation (12). We compared the results of numerical solution for (10) by the shooting method with the well known analytical solution for a rectangular quantum well.[28] It was found that the mesh size of about 1500 points yields quite good accuracy with a relative error in eigenvalue determination less than 10^{-3} for almost all levels.

After the set of eigenvalues E_i and corresponding eigenvectors $\psi_i(z)$ had been obtained, the carrier concentration in the QW region was calculated via local density of states from the expression[21,25]

$$n(z) = \frac{m^*(z)kT}{\pi\hbar^2}\sum_i \ln\left[1+\exp\left(\frac{E_F - E_i}{kT}\right)\right]|\psi_i(z)|^2, \quad (14)$$

using the condition of normalizing the wave functions

$$\int_{-\infty}^{+\infty} |\psi_i(z)|^2 dz = 1. \quad (15)$$

Summation in (14) runs over all subbands.

The prefactor in expression (14) before the square of wave function is considered as the number of electrons per unit area in the ith subband.

As was noted, in the quantum well region the total concentration of electrons was calculated from the Schrödinger equation. We consider this a more correct approach than the simple summation of bound (inside QW) and free carriers (above QW) used, for example, in Ref. 21. But, due to the finite width of the quantum box the continuum of free electron states in this scheme of computations is represented by a set of discrete levels with energies determined by the size of the quantum box.

In order to sum up all charge carriers in the quantum well region we took into account the 16 lowest energy levels. Figure 5 shows the occupation of the 16 energy subbands at different bias. The carrier concentration in the first subband n_1 was at least ten times greater than in the second one, and the concentration in 16th subband (and all higher subbands) is below 10^{-7} of n_1 and can be neglected.

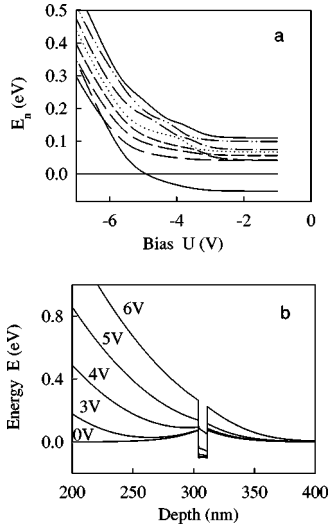

FIG. 6. Results of numerical calculations for sample #300 (x =0.23; well width=7.2 nm; offset ΔE_C=175 meV); T=300 K: (a) first 8 energy levels as function of U_{rev}; (b) the conduction band bottom near the QW at different U_{rev}.

The results of the computation of energy states against applied reverse bias for the sample #300 (ΔE_C=175 meV) are shown in Fig. 6(a), and the lineup of the conduction band bottom for this structure is depicted in Fig. 6(b). As can be seen, a single bound level is observed in the structure with the energy 49 meV in equilibrium. (The bottom of the conduction band in the electroneutrality region was taken as zero.) Starting approximately at −2.5 V the space charge regions of the Schottky barrier and the QW merge (Fig. 7), and the penetrating electric field bends the conduction band bottom near the QW, forcing the bound level to lift up. At U =−5 V the level becomes unbound.

To calculate the C-V characteristics the "quasistatic approach" [29] was applied. The capacitance of a structure is the first derivative of its total charge. The latter can be derived via the flow of electric field across the surface according to Gauss theorem. The spatial distribution of electrostatic potential φ is calculated during solution of the Poisson equation, so one can derive the electric field at the surface at every applied bias

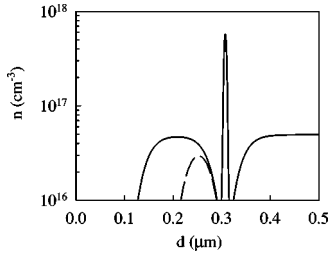

FIG. 7. Simulated concentration profiles of electrons in the region of QW at U=−1 V (solid) and −2.5 V (dashed line), T =300 K. Sample #300.

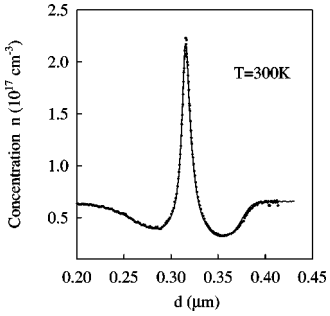

FIG. 8. Experimental (dots) and fitted (solid) apparent concentration profiles of $In_{0.23}Ga_{0.77}As/GaAs$ quantum well (sample #300). Best fit with $\Delta E_C = 175$ meV.

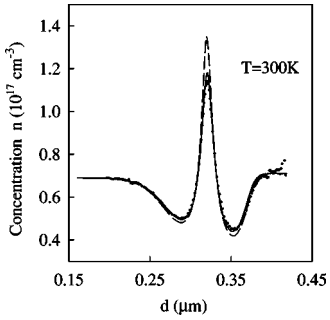

FIG. 9. Resolution of the fitting. The results for the best fit ($\Delta E_C = 120$ meV, solid line) and for $\Delta E_C = 130$ meV (dashed line) are presented. Dotted curve, the experimental apparent profile for sample #303 ($x = 0.145$).

$$E_{\text{surf}} = \frac{\varphi_1 - \varphi_0}{h_{\text{barr}}}, \tag{16}$$

and, hence, build up the capacitance-voltage characteristic (or restore the apparent concentration profile) using (1). Here, φ_0 and φ_1 are the calculated potentials in the finite-difference mesh of the Poisson equation just at the Schottky barrier and nearest to it.

IV. RESULTS OF SIMULATION AND DISCUSSION

As has been established earlier,[20,30] there exists a certain discrepancy between the true and "apparent" concentration profiles of free charge carriers near a heterojunction, quantum well or quantum dot.[31–33] An apparent profile, obtained in experiment, is more smeared in comparison to the true one and has a shift in the peak position (see Fig. 4). The general reason for this discrepancy is the indirect and nonequilibrium procedure of concentration profile restoration from *C-V*-measurements. Generally, this technique involves differentiation of the *C-V*-curve (1) in the approximation of fully depleted space charge region and does not take into account the problem of Debye smearing. In the case of QW profiling, where one expects "sub-Debye resolution," this standard technique leads to an essential distortion of the apparent profile. So, for the goal of adequate fitting, during simulations we must accomplish just the same procedure of restoration of the apparent profile as in real experiments and, particularly, the bias voltage increment in the simulation must be equal to the voltage step used in the experiment.

The results of fitting for two samples are presented in Figs. 8 and 9. As can be seen, excellent matching is obtained. This proves the correctness of the used model. One should underline again that due to the high quality of the specially fabricated for *C-V*-measurements samples no additional adjustable parameters like an impurity concentration gradient or a charge at the heterojunction had to be used in the fitting procedure. The only fitting parameter was the conduction band offset, ΔE_C. The value of majority carrier concentration was taken on the shoulders of the measured concentration profiles. Parameters for $In_xGa_{1-x}As$, needed for the calculations, were taken from Refs. 26 and 34. Figure 9 also demonstrates the resolution of our fitting. For a medium In-content ($x = 0.14$) the error was less than 10 meV. It was found that the resolution is approximately directly proportional to the alloy composition of the quantum well. In general, assuming normal (Gaussian) function of errors,[35] we estimate the relative error in the determination of a band offset as less than 10% with the probability $\alpha = 0.997$ within the measured range of x.

An interesting example of fitting for the sample with the smallest In-content in QW ($x = 0.065$, sample #298) is presented in Fig. 10. Here the apparent peak of enrichment in the QW is even smaller than the doping concentration, despite the spatial confinement inside the QW. The simulated profile in this case is very sensitive to the band offset (the error is about 5 meV), however, the fitting is not as good as for other compositions. For such a weak concentration peak the presence of residual impurities in the quantum well and in adjacent spacers begins to play an essential role. One also should bear in mind the increased relative value of the experimental noise.

In Table I we have summarized the conduction band offsets in strained pseudomorphically grown $In_xGa_{1-x}As/GaAs$ ($0.06 \leqslant x \leqslant 0.29$) quantum wells obtained in our study. Only one bound level was observed in all samples. Its depth in equilibrium ($U = 0$ V) is depicted in Fig. 11 as a function of composition. One can see that for compositions $x < 0.25$ the level appears above the corresponding Fermi level. Nevertheless, the occupation in the subband remains significant to provide an excess of apparent carrier concentration in QW region over the dopant value in all samples, except for $x = 0.065$.

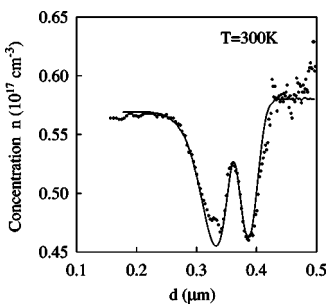

FIG. 10. Apparent concentration profile of $In_xGa_{1-x}As/GaAs$ quantum well with low In-content $x_{In} = 0.065$ (dotted) and fitted curve (solid) with $\Delta E_C = 55$ meV (sample #298).

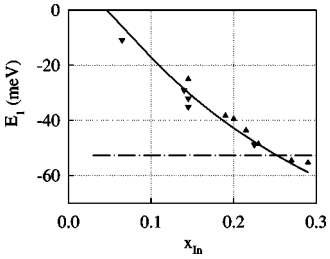

FIG. 11. Position of bound energy level E_1 in strained $In_xGa_{1-x}As/GaAs$-QWs (triangles up for $w \leqslant 7.2$ nm and triangles down for $w > 7.2$ nm). Solid line, calculated dependence E_1 of x_{In} in the assumption $w = 7.2$ nm and for the impurity doping as in the sample #300. Dashed-dotted line, the corresponding position of the Fermi level.

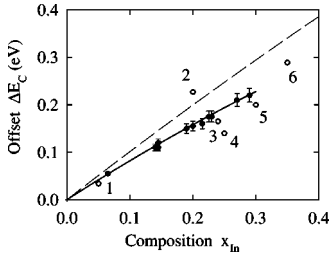

FIG. 12. Conduction band offsets in strained $In_xGa_{1-x}As/GaAs$ QWs as function of composition. Errors bars correspond to the 95% confidence interval. Dashed line, as recommended in Ref. 9. Open circles, the last decade results of capacitance and optical investigations on strained $In_xGa_{1-x}As/GaAs$-QWs: 1, Ref. 38; 2, Ref. 14; 3, Ref. 19; 4, Ref. 18; 5, Ref. 13; 6, Ref. 11.

From Fig. 11 it can be seen that there is no bound energy level for $x < 4\%$. It turns into the resonant one, since the decreasing well depth becomes comparable to the conduction band bending [see Fig. 6(b)]. Besides that, the weak doping in adjacent with QW spacers leads to additional band bending near the QW, which lifts the energy level up.

In Fig. 12 the results on conduction band offsets in strained $In_xGa_{1-x}As/GaAs$-QWs obtained during the numerical fitting to the experimental *C-V* characteristics are presented. The "recommended" curve from the above mentioned review[9] is also depicted. The "recommended" band offsets are higher by about 25% in comparison to our results for strained quantum wells. The origin of this difference, as it was mentioned above, is the presence of elastic strains in thin InGaAs layer, pseudomorphically grown on GaAs substrate. Estimations on the base of model-solid theory[36] predict the increase of the band gap of compressively strained InGaAs in comparison to the value ΔE_g for bulk material again at the order 25%. So, the absolute values of band discontinuities are smaller in compressively strained quantum wells than in relaxed single heterostructures or thick double heterostructures. Within the pseudomorphical growth of quantum well the band offset is independent on the alloy thickness. At approaching to the critical layer thickness [~20 nm for $x = 0.23$ (Ref. 37)], one should expect the violation of the law because of significant increase of misfit dislocations. But, on the other hand, the layers with thickness 20 nm (for $x = 0.23$) and greater are beyond the practical interest, since in such quantum wells several bound energy states with close energies do arise due to the decreasing of quantization effects. Hence, for the practical case of devices on strained quantum well the expression obtained here may be considered as universal. Recent results of other researchers on strained QWs, mainly obtained by capacitance techniques (also depicted in Fig. 12), are in reasonable agreement with ours, but exhibit essential scattering.

The experimentally obtained dependence $\Delta E_C = f(x)$ is close to a straight line with only little bowing. When fitting the curve to a parabola we took into account the different absolute errors in band offset determination for different compositions x using the covariance matrix (matrix of errors).[35] Thus, we propose the expression $\Delta E_C(x) = 0.85x - 0.3x^2$ for the conduction band offsets in strained $In_xGa_{1-x}As/GaAs$ quantum wells in the composition range $0 < x < 0.3$.

V. SUMMARY

Aiming to get the accurate and precise values for conduction band offsets, a set of high quality samples containing strained $In_xGa_{1-x}As/GaAs$ quantum wells was grown in the composition range $0.06 \leqslant x \leqslant 0.29$. Specially for *C-V*-measurements a constant impurity concentration in the cladding layers was maintained during the growth in order to eliminate uncertainties in subsequent numerical simulations. A fitting procedure for experimentally obtained apparent concentration profiles has been implemented using the self-consistent solution of Schrödinger and Poisson equations. All important information about the properties of the quantum well heterostructures was derived: the majority carrier profiles, the positions of energy levels, corresponding wave functions for electrons, profile of the conduction band bottom, as well as the dependencies of the above mentioned parameters on the applied electric field. The presence of only one bound level was discovered in all samples. It was found that the conduction band offsets in strained $In_xGa_{1-x}As/GaAs$ quantum wells follow the expression $\Delta E_C(x) = 0.85x - 0.3x^2$.

*Electronic address: vizubkov@mail.eltech.ru

[1] R. Dingle, W. Wiegmann, and C. H. Henry, Phys. Rev. Lett. **33**, 827 (1974).
[2] R. Dingle, A. C. Gossard, and W. Wiegmann, Phys. Rev. Lett. **34**, 1327 (1975).
[3] H. Kroemer, Surf. Sci. **132**, 543 (1983).
[4] H. Kroemer, J. Vac. Sci. Technol. B **2**, 433 (1984).
[5] H. Kroemer, Surf. Sci. **174**, 299 (1986).
[6] G. Duggan, J. Vac. Sci. Technol. B **3**, 1224 (1985).
[7] E. T. Yu, J. O. McCaldin, and T. C. McGill, Solid State Phys. **46**,

1 (1992).
[8] B. Jogai and P. W. Yu, Phys. Rev. B **41**, 12 650 (1990).
[9] I. Vurgaftman, J. R. Meyer, and L. R. Ram-Mohan, J. Appl. Phys. **89**, 5815 (2001).
[10] *Properties of Lattice-Matched and Strained Indium Gallium Arsenide*, edited by P. Bhattacharya (INSPEC, London, 1993).
[11] J. Arias, I. Esquivias, E. C. Larkins, S. Bürkner, S. Weisser, and J. Rosenzweig, Appl. Phys. Lett. **77**, 776 (2000).
[12] P. Disseix, J. Leymarie, A. Vasson, A.-M. Vasson, C. Monier, N. Grandjean, M. Leroux, and J. Massies, Phys. Rev. B **55**, 2406 (1997).
[13] G. Karunasiri, J. Appl. Phys. **79**, 8121 (1996).
[14] L. Lu, J. Wang, Y. Wang, W. Ge, G. Yang, and Z. Wang, J. Appl. Phys. **83**, 2093 (1998).
[15] S.-H. Wei and A. Zunger, Appl. Phys. Lett. **72**, 2011 (1998).
[16] F. Bugge, U. Zeimer, M. Sato, M. Weyers, and G. Tränkle, J. Cryst. Growth **183**, 511 (1998).
[17] J. H. Davies, *The Physics of Low-Dimensional Semiconductors: An Introduction* (Cambridge University Press, Cambridge, 1998).
[18] X. Letartre, D. Stievenard, and E. Barbier, Appl. Phys. Lett. **58**, 1047 (1991).
[19] S. Subramanian, B. M. Arora, A. K. Srivastava, G. Fernandes, and S. Banerjee, J. Appl. Phys. **74**, 7618 (1993).
[20] B. M. Tschirner, F. Morier-Genoud, D. Martin, and F. K. Reinhart, J. Appl. Phys. **79**, 7005 (1996).
[21] P. N. Brounkov, T. Benyattou, and G. Guillot, J. Appl. Phys. **80**, 864 (1996).
[22] S. M. Sze, *Physics of Semiconductor Devices*, 2nd ed. (Wiley, New York, 1981).
[23] F. Stern, Phys. Rev. B **5**, 4891 (1972).
[24] F. Stern and S. D. Sarma, Phys. Rev. B **30**, 840 (1984).
[25] I.-H. Tan, G. L. Snider, L. D. Chang, and E. L. Hu, J. Appl. Phys. **68**, 4071 (1990).
[26] S. Adachi, *Physics Properties of III-V Semiconductors Compounds* (Wiley, New York, 1992).
[27] A. Abou-Elnour and K. Schuenemann, J. Appl. Phys. **74**, 3273 (1993).
[28] L. D. Landau and E. M. Lifshitz, *Quantum Mechanics* 3rd ed. (Pergamon, New York, 1977).
[29] W. C. Johnson and P. T. Panousis, IEEE Trans. Electron Devices **ED-18**, 965 (1971).
[30] H. Kroemer, W.-Y. Chien, J. J. S. Harris, and D. D. Edwall, Appl. Phys. Lett. **36**, 295 (1980).
[31] P. N. Brunkov, A. A. Suvorova, M. V. Maximov, A. F. Tsatsul'nikov, A. E. Zhukov, A. Y. Egorov, A. R. Kovsh, S. G. Konnikov, T. Inn, S. T. Stoddart *et al.*, in *International Symposium on Nanostructures: Physics and Technology*, St. Petersburg, 1997, p. 236.
[32] C. M. A. Kapteyn, F. Heinrichsdorff, O. Stier, R. Heitz, M. Grundmann, N. D. Zakharov, D. Bimberg, and P. Werner, Phys. Rev. B **60**, 14265 (1999).
[33] V. I. Zubkov and A. V. Solomonov, in *International Symposium on Nanostructures: Physics and Technology*, St. Petersburg, 2001, pp. 244–247.
[34] *Ternary and Quaternary III-V Compounds*, Vol. 2 in *Handbook Series on Semiconductor Parameters*, edited by M. Levinshtein, S. Rumyantsev, and M. Shur (World Scientific, London, 1999).
[35] D. J. Hudson, *Statistics* (Geneva, 1964).
[36] C. G. Van de Walle, Phys. Rev. B **39**, 1871 (1989).
[37] Ch. Köpf, H. Kosina, and S. Selberherr, Solid-State Electron. **41**, 1139 (1997).
[38] M. J. Joyce, Z. Y. Xu, and M. Gal, Phys. Rev. B **44**, 3144 (1991).